npj Climate and Atmospheric Science https://doi.org/10.1038/s41612-026-01341-8

Article in Press

The relationship between the origin of tropical cyclones and their maximum attained intensity

Received: 27 October 2025

Accepted: 23 January 2026

Cite this article as: Xiao, R., Wu, L., Gong, Z. *et al.* The relationship between the origin of tropical cyclones and their maximum attained intensity. *npj Clim Atmos Sci* (2026). https://doi.org/10.1038/s41612-026-01341-8

Ruotong Xiao, Liang Wu, Zhiqiang Gong, Zhiping Wen, Tao Feng, Xi Cao & Shangfeng Chen

The relationship between the origin of tropical cyclones and their maximum attained intensity

Ruotong Xiao[1,2,3], Liang Wu[3,1] *, Zhiqiang Gong[2], Zhiping Wen[1,4], Tao Feng[5], Xi Cao[3], Shangfeng Chen[3]

[1] Department of Atmospheric and Ocean Sciences & Institute of Atmospheric Sciences/Shanghai Key Laboratory of Ocean-land-atmosphere Boundary Dynamics and Climate Change, Fudan University, Shanghai, China.

[2] Chinese Academy of Meteorological Sciences, China Meteorological Administration, Beijing, China.

[3] National Key Laboratory of Earth System Numerical Modeling and Application/Center for Monsoon System Research, Institute of Atmospheric Physics, Chinese Academy of Sciences, Beijing, China.

[4] Institute of Eco- Chongming (IEC), Shanghai, China.

[5] Key Laboratory of Marine Hazards Forecasting/College of Oceanography, Hohai University, Nanjing, China.

*Corresponding author:

Prof. Liang Wu, Institute of Atmospheric Physics, Chinese Academy of Sciences, P. O. Box 9804, Beijing 100029, China.

E-mail: wul@mail.iap.ac.cn

Abstract

Most tropical cyclones (TCs) originate from tropical disturbances over the western North Pacific (WNP). This study examines the tropical disturbances that developed into TCs and their relationship with maximum attained intensity. Using data from 1981 to 2020, we reveal that 29.1% of developing disturbances originated from Mixed Rossby–Gravity (MRG) waves. Compared with other origins, MRG-originated TCs intensify faster, produce more super typhoons, and reach higher lifetime maximum intensity (LMI). These developing systems typically form farther southeast and follow prolonged northwestward tracks, benefiting from a longer pre-LMI oceanic trajectory and greater exposure to favorable large-scale conditions, including warmer sea surface temperature, greater mid-level moisture, stronger convection and weaker vertical wind shear. Following their formation, the disturbances co-propagate westward with the MRG wave packet, which itself does not dissipate. 81.8% of these disturbances remain within the MRG wave packet until reaching their LMI, for an average duration of 3.7 days. The MRG wave packet provides favorable conditions for disturbance development, including warmer sea surface temperatures, enhanced moisture supply, reduced vertical wind shear, and stronger upper-level divergence—features that collectively promote intensification. Furthermore, the proportion of TCs statistically associated with MRG-related disturbances shows a significant increasing trend, underscoring an increasingly important role of MRG wave environments in modulating TC intensity.

Introduction

Tropical cyclones (TCs) are among the most destructive weather phenomena on earth, causing catastrophic rainfall, extreme winds, and coastal inundation. Under global warming, the frequency of intense TCs has increased significantly[1–4]. The impact of TCs critically depend on their lifetime maximum intensity (LMI)[5], which can be influenced by various factors throughout their life cycle, including genesis conditions[6–8], environmental interactions and internal dynamics[9–17]. Although some progress has been made in predicting TC intensity using dynamical models, statistical studies exploring the factors that control the LMI of TCs remain limited[6–8].

Evidence suggests that developing disturbance/TC geneses are critical in determining their eventual intensity. Previous research has established links between genesis conditions and LMI through case studies and numerical models[6,7,18]. For example, Rappin et al.[7] found that tropical disturbances with stronger tangential winds or lower central pressures at the time of their generation are more likely to develop into stronger TCs. Focusing on North Atlantic TCs, Ditchek et al.[6] examined their LMI and identified key genesis variables, such as lower-level vortex strength and mid-tropospheric vorticity, which demonstrate a strong correlation with LMI. Additionally, Lu and Tang[18] applied machine learning and composite analysis to demonstrate that a more compact low-level vortex during the early stages of TC development enhances intensification, leading to a higher LMI by promoting a stronger, more organized circulation. While previous studies have suggested that the origin of tropical disturbances can influence the LMI of TCs, the key factors, the climatological statistics relationship and the underlying mechanisms remain to be

explored. This is particularly true for the western North Pacific (WNP), where TCs are shaped by highly complex environmental conditions such as monsoon troughs, monsoon gyres, and tropical waves.

Previous studies have shown that most TCs originate from pre-existing tropical disturbances[19,20]. Over the WNP, approximately 80% of these disturbances are associated with equatorial tropical waves[21–24]. Among the various wave types, Mixed Rossby–Gravity (MRG) waves have been identified as a particularly influential background[22,23,25]. MRG waves are characterized by westward phase propagation and eastward group velocities. They do not radiate wave energy westward. Instead, their evolution can involve scale contraction and structural transformation under the influence of background flow and monsoon-related shear, leading to the emergence of smaller-scale disturbances embedded within the wave packet[26–28]. These embedded disturbances do not represent a westward radiation of MRG wave energy, but rather arise from internal scale transformation and wave–flow interaction during the westward phase propagation of the parent MRG wave. Such smaller-scale disturbances can often serve as effective precursors for tropical cyclogenesis under favorable environmental conditions, accounting for nearly 30% of TC genesis events over the WNP[21,24]. Feng et al.[21] demonstrated that the phase relationship between pre-TC vortices and the associated tropical waves significantly influences disturbance intensity development. In-phase interactions between the disturbance and the wave favor a rapid intensification of tropical disturbance, while out-of-phase interactions tend to suppress it. This modulation likely occurs by altering the local thermodynamic and kinematic conditions through the equatorial wave environment, thereby affecting the disturbance's development potential. Such

interactions suggest that the origin of a TC within specific tropical wave structures, such as MRG waves, can have a profound impact on its intensity evolution. However, the quantitative linkages between MRG-originated tropical disturbances and TC LMI remain largely unexplored.

While research on TC genesis and development is well-established, the specific influence of MRG-originated TC genesis on subsequent TC intensity has not yet been fully addressed. This study assesses the statistical relationship between the TC origin from MRG waves and the LMI of TCs, providing new insights for TC intensity prediction. Through a comparative analysis of TC characteristics and the environmental conditions associated with MRG waves, this study investigates: (1) the differences in genesis location, track characteristics, life cycle evolution, and LMI between MRG-originated and non-MRG-originated TCs; and (2) the physical mechanisms by which MRG waves modulate TC intensity, including the genesis environment, track steering, and wave–vortex interactions.

Results

Contribution of MRG waves to TC genesis and spatial distribution

A total of 958 TC genesis events is recorded in the WNP region (0°–30°N, 120°E–180°) during 1981 and 2020. Pre-existing tropical disturbances contribute to 79.0% of these TCs. MRG waves are a significant source of disturbances leading to TC formation, as previous studies have confirmed the critical role of this transformation[27,28,45–47]. A total of 279 out of the 757 developing disturbances are associated with MRG wave signals at their initial time, accounting for 29.1% of all TCs (Fig. 1a). In contrast, 478 developing disturbances are not associated with MRG waves at

genesis, making up 49.9% of the total TCs. Notably, the spatial distribution of genesis locations for MRG-originated and non-MRG-originated TCs differs significantly. TCs originating from MRG wave typically form further southeast (Fig. 1b), whereas TCs originating from non-MRG wave exhibit a peak genesis location near 130°E, east of the Philippines, and a secondary peak in the SCS. TCs without precursor disturbances are predominantly concentrated in the SCS, likely reflecting the local characteristics of SCS TCs[31]. Because the SCS represents a semi-enclosed basin with environmental conditions and genesis mechanisms distinct from the broader WNP, our analysis focuses on disturbances developing over the open WNP and does not further examine locally formed SCS TCs. Note that current research primarily focuses on the origin of developing disturbances. The number of MRG-originated TCs shows a negative correlation with the number of TCs that do not originate from MRG waves (correlation coefficient = -0.24, significant at the 90% confidence level). Despite a decrease in the total number of developing disturbances, MRG-originated disturbances have increased slightly. Consequently, the proportion of MRG-originated TCs relative to total TCs has exhibited a significant upward trend from 1981 to 2020 (Fig. 1c). We note that the diagnosed increase in the fraction of MRG-originated TCs exhibits pronounced interannual variability, partly linked to ENSO modulation. Importantly, after excluding moderate-to-strong ENSO years, the upward trend in the fraction of MRG-originated TCs persists and remains statistically significant (Supporting Information Fig. S1), indicating that the diagnosed trend is not solely driven by ENSO clustering.

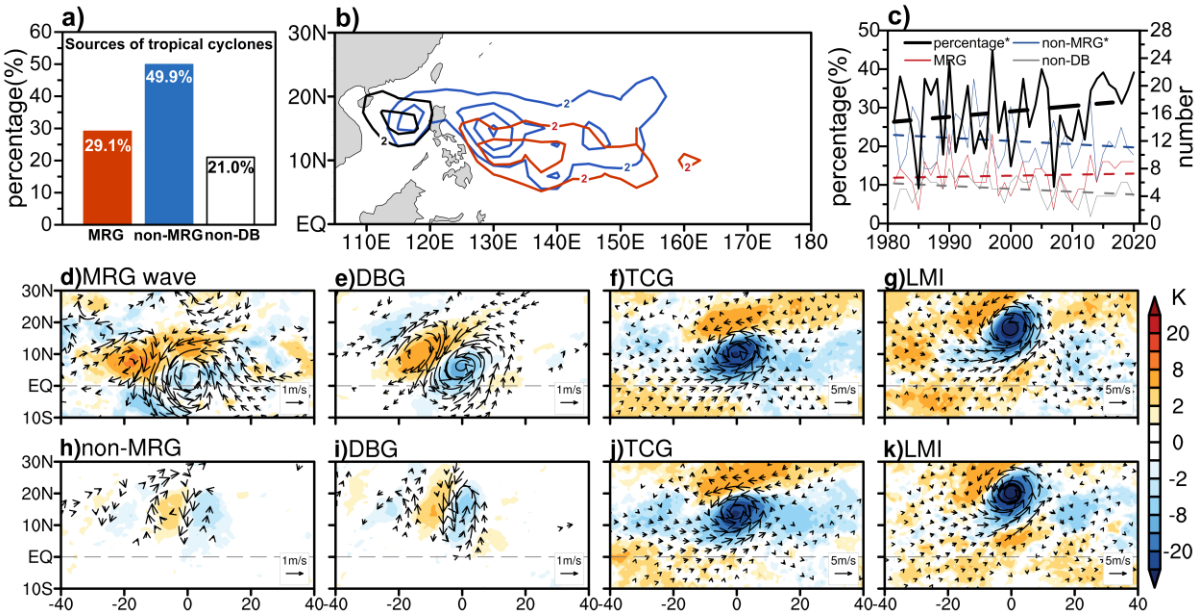

Structural and intensity differences

Tropical disturbances of different origins exhibit distinct wind field and convective structures at various stages of disturbance development (Figs. 1d-k). The clear differentiation in physical characteristics between MRG-originated and non-MRG-originated disturbances validates the effectiveness of our identification method. The disturbances originating from MRG waves display a classic MRG wave pattern on the day preceding genesis, characterized by an equatorially symmetric, counterclockwise-rotating low-level vortex accompanied by an equatorially antisymmetric distribution of convection. In this convection region, intense updrafts and deep convection are often associated with the strengthening of the low-level vortex. MRG waves propagate westward near the equator, with the vortex and convective activity tightly coupled during this evolution (Fig. 1d). As the disturbance develops, the vortex gradually intensifies, and the convection begins to align with the low-level vortex center (Fig. 1e), forming more concentrated updrafts and deep convection. At this stage, the vortex and convection remain tightly

coupled, marking a successful genesis of tropical disturbance. The disturbance then begins to move northwestward, laying the foundation for subsequent TC formation (Fig. 1f).

In contrast, non-MRG-originated disturbances typically show weaker intensification (Figs. 1h, i) and lack prominent circulatory features in their early stages (Fig. 1h). Since the TC data at genesis time exhibit similar intensities, the low-level vortex structures and intensities at the time of genesis are similar for both disturbance types (Figs. 1f, j). However, significant differences in wind speed and convective structure become apparent when they reach their LMI. MRG-originated TCs exhibit a more pronounced cyclonic circulation and more organized convection within the storm center compared to non-MRG-originated TCs (Figs. 1g, k). It should be noted that the composite circulation patterns are sensitive to the spatial distribution of the contributing events. The broader meridional spread of non–MRG-associated TCs tends to smear out the circulation signal in the composite fields, making the gyres appear more poleward-elongated and weaker than those of MRG-associated TCs. This effect reflects compositing characteristics rather than weaker intensities of individual storms, which are instead quantified using event-based LMI statistics.

MRG-originated TCs achieve a mean LMI of 46.76 m s^{-1}, which is significantly higher than 42.89 m s^{-1} observed for non-MRG-originated TCs, representing a 9.0% increase in LMI. This difference is statistically significant at the 99% confidence level (Fig. 2a). At the time of LMI, the horizontal distribution of the 850-hPa wind field and Tb differences shows that MRG-originated TCs possess stronger low-level cyclonic circulation and convective activity, with maximum differences of 2.7 m s^{-1} in wind speed and 5.9 K in Tb compared to non-MRG-originated TCs (Fig. 2b). In other words, TCs originating from MRG waves typically have higher intensities. This

difference tends to be apparent when LMI reach 35 m s^{-1} (Fig. 2c). When the LMI is above 55 m s^{-1}, the number of MRG-originated TCs significantly increases compared to non-MRG-originated TCs. 75.64% of MRG-originated TCs develop into typhoons (TY), with 49.45% becoming super typhoon (Super TY). These proportions greatly exceed those of non-MRG-originated TCs, of which only 52.98% attain TY intensity and 32.03% become Super TYs (Fig. 2c).

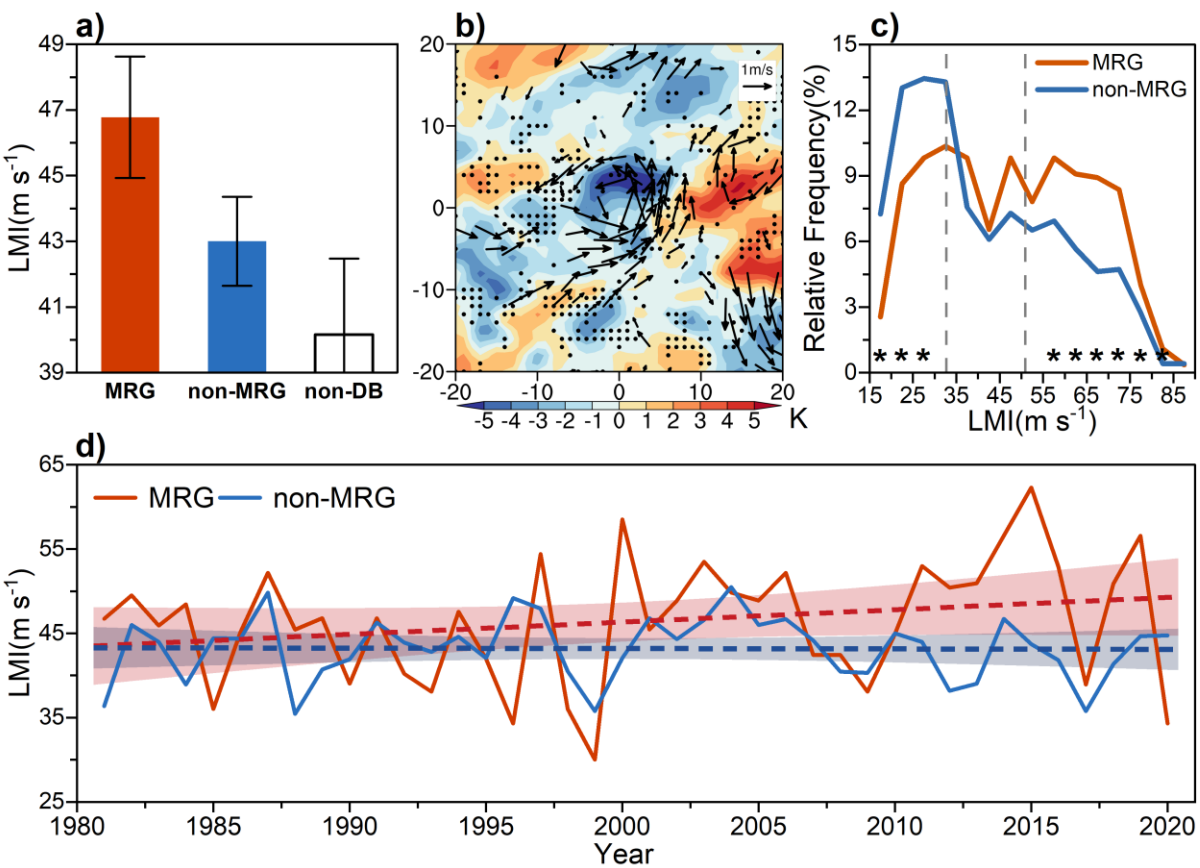

Notably, the annual frequency of non-MRG-originated TCs is declining significantly (Fig. S1), which is consistent with the decrease in overall TC frequency reported in previous studies[48]. In contrast, the frequency of MRG-originated TCs shows no clear trend. However, their proportion relative to the total TCs has increased significantly. The differences between the year-mean LMI of MRG-originated TCs and non-MRG-originated TCs are relatively small in the early stages, but

after 2000, the disparity becomes more pronounced. During this later period, MRG-originated TCs display a significant upward trend in LMI (Fig. 2d), whereas non-MRG-originated TCs show no notable change in LMI intensity. A similar ENSO sensitivity is found for the long-term variation of LMI (Fig. 2d). After masking moderate and strong ENSO years, the increasing tendency of LMI for MRG-originated TCs remains detectable (Supporting Information Fig. S2). This indicates that ENSO plays an important role in modulating the interannual variability of TC intensity, but does not fully account for the observed long-term tendency. Taken together, the persistence of the increasing LMI tendency after masking ENSO years, along with the increasing fraction of TCs statistically associated with MRG-related disturbances, indicates that MRG waves may be involved in modulating disturbance genesis and early development. This influence, operating

alongside ENSO-related variability and other processes, may contribute to variations in TC intensity.

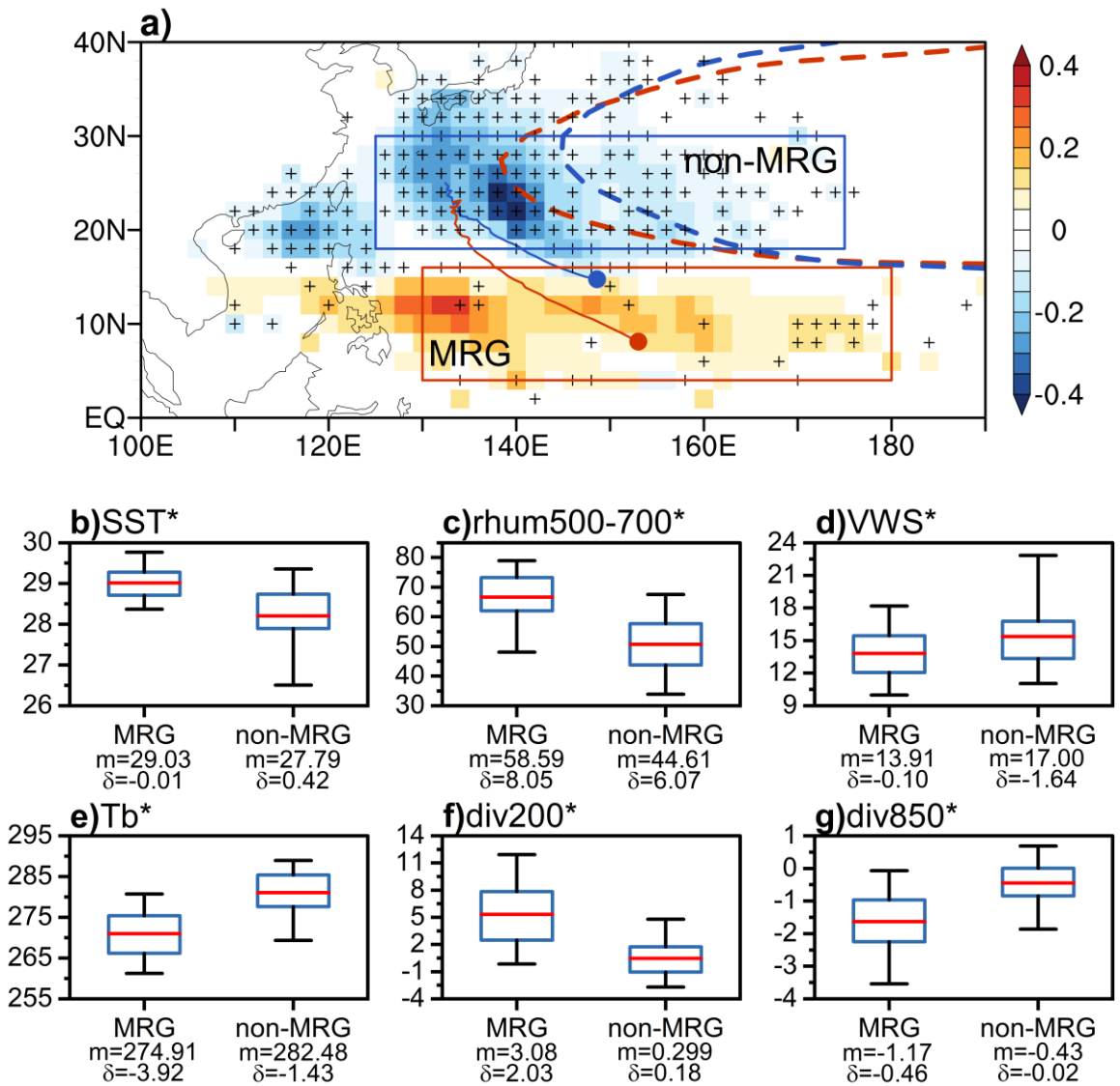

Environmental modulation and persistence of MRG wave influence during cyclone development

Significant differences exist in the activity regions of the MRG-originated and non-MRG-originated disturbances and their subsequent evolution (Fig. 3a). Disturbance track density and

genesis locations are closely tied to the initial genesis position[49,50] and to the large-scale steering flow[51,52]. First, the two origins show distinct mean genesis locations and track bands. MRG-originated disturbances form farther southeast and propagate at lower latitudes (0–10°N), ranging from the Philippine Sea to the central-eastern WNP (Figs. 1b, 3a). By contrast, non-MRG-originated disturbances have a mean genesis position ~6.7° farther north and track predominantly through subtropics (15°–30°N, 125°–165°E) and the SCS (5–25°N, 110–120°E). The spatial distributions of the two partially overlap with the regions of the ITCZ/monsoon trough. However, in this study, the ITCZ/monsoon trough is treated as a low-frequency background state, while MRG waves are analyzed from a wave-dynamical perspective. Although interactions between MRG waves and the ITCZ/monsoon trough are expected in the real atmosphere, explicitly diagnosing such interactions is beyond the scope of the present analysis. Second, during development, MRG-originated disturbances and their ensuing tracks are associated with a stronger, more westward subtropical ridge. This westward displacement causes the northward steering flow to shift accordingly, prompting MRG-originated systems to initiate their poleward turn at more western longitudes. Consequently, these systems spend more time south of 15°N, resulting in a substantially longer pre-LMI oceanic trajectory for about 768 km on average (Supporting Information Fig. S3) and a correspondingly longer duration over warm ocean compared to their non-MRG-originated counterparts.

To further investigate the effect of latitudinal variation of disturbance and TC activity on its LMI, the aforementioned analysis domain is divided into two sub-regions (Fig. 3a): the MRG region (4°N-16°N, 130°E-180°E) and the non-MRG region (18°N-30°N, 125°E-175°E). This

division allows for a detailed comparison of the environmental conditions that influence TC development in regions dominated by different types of disturbances, namely MRG-dominated and non-MRG-dominated disturbances. Using 20-day low-pass filtered data to minimize the influence of TC themselves (Figs. 3b-g), we conduct a comparative analysis of key background environmental parameters, averaged over the period of disturbance and TC development (Fig. 3a). These parameters are averaged over the disturbance life cycle (Fig. 3a) for each region, allowing for a clear comparison of the conditions across the two sub-regions. This MRG-dominated region exhibits: reduced vertical wind shear, higher SST, deeper moisture-rich layers (especially 500-700 hPa), stronger upper-level divergence, low-level convergence and upward motion. The combination of these factors creates a more favorable thermodynamically and dynamically environment, promoting the development of MRG disturbances into TCs with stronger peak intensities.

At the same time, analysis of the deviation between the disturbance life cycle and the regional climate average further reveals that, although the non-MRG region remains conducive to TC development, it generally lacks the pronounced intensity-enhancing characteristics of the MRG-dominated region. For instance, although the non-MRG region has SST higher than the environmental average, its overall SST is lower than that of the MRG region. Similarly, moisture content, vertical wind shear, Tb, and upper- and lower-level convergence and divergence show similar patterns. Overall, the environmental differences between the MRG and non-MRG regions provide valuable insights into the role of disturbance origin in shaping the TC intensity. It is important to note that all storms examined in this study are TCs governed by the same fundamental

internal dynamics. The LMI differences identified here do not imply distinct TC types, but instead reflect differences in large-scale environmental modulation associated with disturbance origin and subsequent wave–environment coupling.

In addition, it is notable that the MRG wave often persists after the development of the disturbance[26,47]. Composite Hovmöller diagrams averaged over 10°S–10°N for all MRG-originated disturbances (Fig. 4a) show that the MRG wave remains present and continues to propagate westward throughout the disturbance and subsequent TC development stages. It should be noted that the westward propagation shown here represents the phase evolution of the MRG wave, while the associated wave energy propagates eastward in a group-velocity sense, consistent with classical MRG wave dispersion.

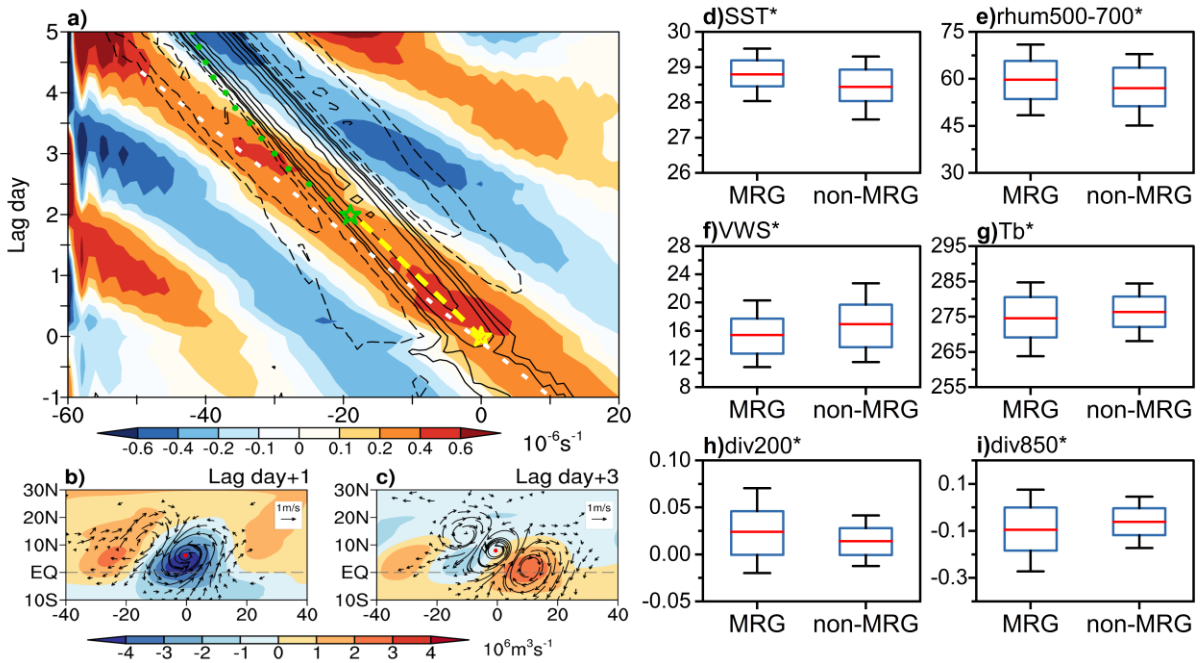

Before the development of a disturbance, the phase evolution of the MRG wave propagates westward at a speed of about 15.9 m s^{-1}, consistent with previous findings[53,54]. As the MRG wave progresses westward, its speed slows slightly, and a developing disturbance forms near the center

of the wave packet (yellow star, Fig. 4a). The nascent disturbance then travels northwestward at roughly 8.9 m s^{-1}. The original MRG signal does not completely dissipate but persists and continues to propagate westward. Under these conditions, the persisting MRG signal overlaps spatially and temporally with the newly emerging disturbance, indicating a coexistence of both wave-disturbance signals. (Figs. 4b, c). On average, the disturbance remains embedded within the MRG wave packet for about two days before transitioning into a TC, which subsequently continues westward at a speed similar to that of the developing disturbance and exits the MRG packet after about 1.6 days. Throughout this period, the MRG wave retains its distinctive characteristics, and both systems co-propagate westward. It should be noted that TCs themselves can excite equatorial wave responses, through energy dispersion processes[55,56]. Therefore, the association between MRG wave signals and TCs does not necessarily imply a purely one-way causal relationship in all cases. In this study, our interpretation is constrained to events in which the MRG wave signal is objectively identified prior to disturbance and TC formation, and the results should be understood as a statistical assessment of the role of pre-existing MRG wave environments in modulating subsequent TC development. We acknowledge that potential two-way interactions between TCs and MRG waves may occur during later stages of storm evolution, but these feedback processes are beyond the scope of the present study.

Composites show that TCs originating from MRG waves are influenced by the MRG packet during their pre-genesis and early development stages for an average of 3.68 days. Upon decoupling from the wave packet, the MRG-originated disturbance reaches a peak wind speed of 39.72 m s^{-1}, 19.6% higher than the 33.2 m s^{-1} for non-MRG-originated disturbances during

equivalent developmental periods. Statistical analysis further indicates that 81.8% of MRG-originated disturbances remain coupled with MRG waves up to their LMI, and that longer coupling durations are associated with higher LMI (correlation coefficient = 0.27, significant at the 99% level; Supporting Information Fig. S4). One possible explanation for this phenomenon is that MRG waves provide a more favorable environment than non-MRG-originated disturbances.

To investigate the environmental conditions provided by MRG waves, we apply a frequency–wavenumber spectral filtering technique to identify the low-level cyclonic circulation (also named as "pouch") of MRG waves at the time of disturbance or TC formation and extract the associated initial environmental fields. To exclude the influence of the disturbance or TC itself, data within a 5° radius of the disturbance center are masked when constructing the environmental fields. For disturbances influenced by MRG waves, we average the pouch-region environmental fields. For non-MRG-originated disturbances, we similarly average the environmental fields within a 15° radius of the disturbance center (comparable to the typical scale of an MRG "pouch").

A systematic comparative analysis of key environmental parameters crucial for TC LMI (Figs. 4d-i) reveals a clear enhancement of favorable conditions within the MRG region compared to non-MRG regions. These include higher SST, reduced vertical wind shear, stronger convection, enhanced upper-level divergence, and intensified low-level convergence—all of which are notably amplified by the MRG wave within the pouch. This MRG environment provides a highly favorable setting for disturbance and TC intensification, far surpassing the potential for such development in the absence of MRG wave forcing. As a result, developing disturbances and TCs that are accompanied by MRG waves experience an average intensity increase rate of 6.17 m s^{-1} per day,

significantly higher than 4.4 m s^{-1} per day for disturbances in the absence of MRG waves. Upon leaving the MRG wave packet, these disturbances reach an average intensity of 39.72 m s^{-1}. Therefore, the persistence of the MRG wave in accompanying a disturbance after its formation plays a critical role in predicting the resulting TC's LMI. Our results demonstrate that continued embedding within the MRG packet supplies a more favorable environment, which explains why MRG-originated TCs attain higher LMIs. This mechanism highlights a potentially predictable pathway linking equatorial wave activity and extreme TC intensity in a warming climate.

Discussion

MRG waves are not only a major source of TC seeds over the WNP but also a key modulator of their peak intensity. This study provides the first comprehensive climatological assessment of how MRG waves influence TC genesis and LMI during 1981–2020. Using 40 years of best-track and reanalysis data combined with wavenumber-frequency filtering, we show that about one third of TCs originate from MRG waves and these systems achieve significantly higher LMIs than non-MRG-originated TCs. MRG-originated disturbances form farther southeast, travel longer over warm waters, and are steered by a stronger, westward-displaced subtropical ridge, providing a longer pre-LMI oceanic trajectory. Its active regions partially overlap with the ITCZ/monsoon trough. Although MRG waves and the monsoon trough are dynamically coupled and can mutually influence each other, as shown in previous studies, the present study adopts a wave-centered perspective and treats the ITCZ/monsoon trough primarily as a low-frequency background state

rather than explicitly analyzing their two-way interactions. The interactions between the two will be discussed in future research.

Composite analyses further reveal that the MRG "pouch" region is characterized by higher SST, deeper mid-level moisture, reduced vertical wind shear, stronger upper-level divergence, and enhanced low-level convergence compared to non-MRG environments. This environment supports an average intensification rate of 6.17 m s^{-1} day^{-1}, compared to 4.4 m s^{-1} day^{-1} in the absence of MRG forcing. Importantly, 82% of MRG-originated disturbances remain coupled with the MRG wave through LMI. Statistical results also indicate that a longer period of co-propagation with the MRG wave packet is associated with a higher LMI. This highlights the importance of wave–vortex coupling in TC intensification.

Together, these findings demonstrate that MRG waves are an important modulator of TC intensity over the WNP. The persistence of the MRG wave in accompanying a disturbance after formation emerges as a key predictor of the eventual LMI, highlighting the potential to incorporate MRG diagnostics into TC intensity forecasts. How MRG waves and the associated TCs respond to future climate forcing remains an open question and represents a limitation of the present study, warranting further investigation in future work using climate model projections.

Methods

Data

TC best-track data are obtained from the International Best Track Archive for Climate Stewardship[29] (IBTrACS, Version 4.0) over the period from 1981 to 2020. The best-track records

provide 6-hourly TC positions (longitude and latitude) and maximum sustained wind speeds. This study only includes TCs that have reached at least tropical storm (TS) intensity, defined by maximum sustained surface winds exceeding 17 m s^{-1}. TC genesis location is defined as the first recorded position of each TC in the dataset[30]. The analysis is conducted in the western North Pacific (WNP; 0–30° N, 120° E–180°) during its TC season spanning from May to November. Tropical disturbances in the South China Sea (SCS) are excluded because their characteristics differ from those over the WNP[31]. Environmental parameters including wind fields, vertical vorticity, relative humidity (rhum) are obtained from the European Centre for Medium-Range Weather Forecasts ERA5[32], with 0.25° × 0.25° spatial resolution and 6-hour temporal resolution. Daily sea surface temperature (SST) data are derived from the NOAA OI SST V2 High Resolution Dataset[33], with the same resolution. Convective activity is assessed using brightness temperature (Tb) data from the Gridded Satellite[34] (GridSat-B1), with 0.07° × 0.07° horizontal resolution every 3 hours. For consistency with other datasets, Tb data are interpolated to a 0.25° × 0.25° grid at 6-hour intervals.

Filtering

The Lanczos filtering technique[35] is used to obtain the synoptic-scale signals at the 2.5-10-day band[36]. The wavenumber-frequency spectral filtering method of Wheeler and Kiladis[37] is applied to isolate the MRG wave signal, with periods of 2.5-10 days, westward wavenumbers 1-10, and equivalent depths of 8 m to 90 m.

Identification and Tracking of Developing Disturbances

Tropical disturbances are often associated with convective activity and vortex coupling. Previous studies[38–42] have highlighted the significance of low-level relative vorticity and convection near the disturbance center as the crucial variables for identifying and tracking tropical disturbances. In this study, we utilize 2–10-day band-pass filtered 850-hPa relative vorticity and Tb data to identify and track tropical disturbances. A disturbance is classified if it displays a cyclonic circulation, with at least one-third of the grid points within a 3° radius showing a filtered relative vorticity greater than 0.2×10^{-5} s^{-1}, a minimum filtered Tb within the same radius lower than -2 K, and a displacement distance not exceeding 5° over a 6-hour period[12,43,44]. If there is a TC recorded in IBTrACS at the next time step (6 h) within a distance of 5° of disturbance's tracked path, it is classified as the developing disturbance of that TC, its trajectory is correspondingly established.

Determining MRG Origin of Developing Disturbances

A disturbance is classified as originating from an MRG wave if, within its initial location, the wavenumber-frequency filtered relative vorticity at 850 hPa exceeds 0.8×10^{-6} s^{-1} during the 6 hours prior to the disturbance's first detection, following the criteria set by Wu and Takahashi[24]. TCs that develop from such disturbances are labeled as MRG-originated for short.

Data availability

The data supporting the findings of the present study are openly available. The IBTrACS data can be accessed at https://www.ncei.noaa.gov/data/international-best-track-archive-for-climate-

stewardship-ibtracs/v04r00/access/netcdf/. The ERA5 data set was acquired via https://doi.org/10.24381/cds.6860a573. The NOAA OI SST V2 High Resolution Dataset was acquired via https://www.psl.noaa.gov/data/gridded/data.noaa.oisst.v2.highres.html. The GridSatB1 data were obtained from the following website: https://www.ncei.noaa.gov/products/gridded-geostationary-brightness-temperature.

References

1. Emanuel, K. Environmental factors affecting tropical cyclone power dissipation. *Journal of Climate* **20**, 5497–5509 (2007).
2. Emanuel, K. Tropical Cyclone Seeds, Transition Probabilities, and Genesis. *Journal of Climate* **35**, 3557–3566 (2022).
3. Knutson, T. R. *et al.* Tropical cyclones and climate change. *Nature Geosci* **3**, 157–163 (2010).
4. Webster, P. J., Holland, G. J., Curry, J. A. & Chang, H.-R. Changes in tropical cyclone number, duration, and intensity in a warming environment. *Science* **309**, 1844–1846 (2005).
5. Kossin, J. P., Knapp, K. R., Olander, T. L. & Velden, C. S. Global increase in major tropical cyclone exceedance probability over the past four decades. *Proc. Natl. Acad. Sci. U.S.A.* **117**, 11975–11980 (2020).
6. Ditchek, S. D., Nelson, T. C., Rosenmayer, M. & Corbosiero, K. L. The Relationship between Tropical Cyclones at Genesis and Their Maximum Attained Intensity. *J. Climate* **30**, 4897–4913 (2017).
7. Rappin, E. D., Morgan, M. C. & Tripoli, G. J. The Impact of Outflow Environment on Tropical Cyclone Intensification and Structure. *Journal of the Atmospheric Sciences* https://doi.org/10.1175/2009JAS2970.1 (2009).

8. Cao, X. *et al.* Characteristics of Barotropic Energy Conversion in Rapid Intensifying and Decaying Tropical Cyclones Over the Western North Pacific. *Geophysical Research Letters* **50**, e2022GL101695 (2023).

9. Fu, B., Peng, M. S., Li, T. & Stevens, D. E. Developing versus nondeveloping disturbances for tropical cyclone formation. Part II: Western north pacific. *Mon. Wea. Rev.* **140**, 1067–1080 (2012).

10. Kilroy, G., Smith, R. K. & Montgomery, M. T. An idealized numerical study of tropical cyclogenesis and evolution at the Equator. *Quart J Royal Meteoro Soc* **146**, 685–699 (2020).

11. Montgomery, M. T., Nicholls, M. E., Cram, T. A. & Saunders, A. B. A Vortical Hot Tower Route to Tropical Cyclogenesis. *Journal of the Atmospheric Sciences* https://doi.org/10.1175/JAS3604.1 (2005).

12. Peng, M. S., Fu, B., Li, T. & Stevens, D. E. Developing versus nondeveloping disturbances for tropical cyclone formation. Part I: North atlantic. *Mon. Wea. Rev.* **140**, 1047–1066 (2012).

13. Shay, L. K., Goni, G. J. & Black, P. G. Effects of a Warm Oceanic Feature on Hurricane Opal. *Mon. Wea. Rev.* **128**, 1366–1383 (2000).

14. Sitkowski, M., Kossin, J. P. & Rozoff, C. M. Intensity and Structure Changes during Hurricane Eyewall Replacement Cycles. *Monthly Weather Review* **139**, 3829–3847 (2011).

15. Smith, R. K. & Montgomery, M. T. Effective buoyancy and CAPE: Some implications for tropical cyclones. *Quart J Royal Meteoro Soc* **148**, 2118–2131 (2022).

16. Wang, Z. Role of cumulus congestus in tropical cyclone formation in a high-resolution numerical model simulation. *Journal of the Atmospheric Sciences* **71**, 1681–1700 (2014).

17. Zhang, W., Fu, B., Peng, M. S. & Li, T. Discriminating Developing versus Nondeveloping Tropical Disturbances in the Western North Pacific through Decision Tree Analysis. *Weather and Forecasting* **30**, 446–454 (2015).

18. Lu, R. & Tang, X. Relationship between Early-Stage Features and Lifetime Maximum Intensity of Tropical Cyclones over the Western North Pacific. *Atmosphere* **12**, 815 (2021).

19. Thorncroft, C. & Hodges, K. African easterly wave variability and its relationship to atlantic tropical cyclone activity. *J. Climate* **14**, 1166–1179 (2001).

20. Zehr, R. M., Branch, R. & Collins, F. Tropical cyclogenesis in the western north pacific. *National Oceanic and Atmospheric Administration* (1992).

21. Feng, X., Yang, G.-Y., Hodges, K. I. & Methven, J. Equatorial waves as useful precursors to tropical cyclone occurrence and intensification. *Nat Commun* **14**, 511 (2023).

22. Frank, W. M. & Roundy, P. E. The Role of Tropical Waves in Tropical Cyclogenesis. *Monthly Weather Review* **134**, 2397–2417 (2006).

23. Schreck, C. J., Molinari, J. & Aiyyer, A. A global view of equatorial waves and tropical cyclogenesis. *Monthly Weather Review* **140**, 774–788 (2012).

24. Wu, L. & Takahashi, M. Contributions of tropical waves to tropical cyclone genesis over the western north pacific. *Clim Dyn* **50**, 4635–4649 (2018).

25. Bessafi, M. & Wheeler, M. C. Modulation of south Indian ocean tropical cyclones by the madden–julian oscillation and convectively coupled equatorial waves. *Monthly Weather Review* **134**, 638–656 (2006).

26. Wu, L., Wen, Z. & Wu, R. Influence of the Monsoon Trough on Westward-Propagating Tropical Waves over the Western North Pacific. Part I: Observations. *Journal of Climate* **28**, 7108–7127 (2015).

27. Wu, L. *et al*. Simulations of the present and late-twenty-first-century western north pacific tropical cyclone activity using a regional model. *Journal of Climate* **27**, 3405–3424 (2014).

28. Dickinson, M. & Molinari, J. Mixed Rossby–Gravity Waves and Western Pacific Tropical Cyclogenesis. Part I: Synoptic Evolution. *J. Atmos. Sci.* **59**, 2183–2196 (2002).

29. Knapp, K. R., Kruk, M. C., Levinson, D. H., Diamond, H. J. & Neumann, C. J. The international best track archive for climate stewardship (IBTrACS): Unifying tropical cyclone data. *Bull. Amer. Meteor. Soc.* **91**, 363–376 (2010).

30. Gu, Y., Wu, L., Zhan, R. & Wen, Z. Climatology of developing and nondeveloping disturbances for tropical cyclone genesis over the western North Pacific. *TAO* **33**, 13 (2022).

31. Wu, L., Zhang, H., Chen, J.-M. & Feng, T. Characteristics of tropical cyclone activity over the south China sea: Local and nonlocal tropical cyclones. *Terr. Atmos. Ocean. Sci.* **31**, 261–271 (2020).

32. Hersbach, H. *et al.* The ERA5 global reanalysis. *Quart J Royal Meteoro Soc* **146**, 1999–2049 (2020).

33. Reynolds, R. W. *et al.* Daily High-Resolution-Blended Analyses for Sea Surface Temperature. *Journal of Climate* **20**, 5473–5496 (2007).

34. Knapp, K. R. *et al.* Globally gridded satellite observations for climate studies. *Bulletin of the American Meteorological Society* **92**, 893–907 (2011).

35. Claude E. Duchon. Lanczos Filtering in One and Two Dimensions. (1979).

36. Wang, Z. & Chen, G. Comparison between Developing and Nondeveloping Disturbances for Tropical Cyclogenesis in Different Large-Scale Flow Patterns over the Western North Pacific. *Journal of Climate* **37**, 655–672 (2024).

37. Wheeler, M. & Kiladis, G. N. Convectively coupled equatorial waves: Analysis of clouds and temperature in the wavenumber–frequency domain. *J. Atmos. Sci.* **56**, 374–399 (1999).

38. Hennon, C. C. *et al.* Tropical Cloud Cluster Climatology, Variability, and Genesis Productivity. https://doi.org/10.1175/JCLI-D-12-00387.1 (2012) doi:10.1175/JCLI-D-12-00387.1.

39. Hsieh, T., Yang, W., Vecchi, G. A. & Zhao, M. Model spread in the tropical cyclone frequency and seed propensity index across global warming and ENSO-like perturbations. *Geophysical Research Letters* **49**, e2021GL097157 (2022).

40. Raavi, P. H. & Walsh, K. J. E. Basinwise statistical analysis of factors limiting tropical storm formation from an initial tropical circulation. *JGR Atmospheres* **125**, e2019JD032006 (2020).

41. Sugi, M. *et al.* Future Changes in the Global Frequency of Tropical Cyclone Seeds. *SOLA* **16**, 70–74 (2020).

42. Wang, Z. Thermodynamic aspects of tropical cyclone formation. *Journal of the Atmospheric Sciences* **69**, 2433–2451 (2012).

43. Gao, S. *et al.* The Role of Latent Heat Flux in Tropical Cyclogenesis over the Western North Pacific: Comparison of Developing versus Non-Developing Disturbances. *JMSE* **7**, 28 (2019).

44. Kerns, B., Greene, K. & Zipser, E. Four Years of Tropical ERA-40 Vorticity Maxima Tracks. Part I: Climatology and Vertical Vorticity Structure. *Monthly Weather Review* **136**, 4301–4319 (2008).

45. Au-Yeung, A. Y. M. & Tam, C.-Y. Dispersion characteristics and circulation associated with boreal summer westward-traveling mixed rossby–gravity wave–like disturbances. *Journal of the Atmospheric Sciences* **75**, 513–533 (2018).

46. Takayabu, Y. N. & Nitta, T. 3-5 day-period disturbances coupled with convection over the tropical pacific ocean. *Journal of the Meteorological Society of Japan* **71**, 221–246 (1993).

47. Wu, L., Wen, Z. & Wu, R. Influence of the monsoon trough on westward-propagating tropical waves over the western north pacific. Part II: Energetics and numerical experiments. *Journal of Climate* **28**, 9332–9349 (2015).

48. Chand, S. S. *et al*. Declining tropical cyclone frequency under global warming. *Nat. Clim. Chang.* **12**, 655–661 (2022).

49. Wu, L., Wen, Z., Huang, R. & Wu, R. Possible linkage between the monsoon trough variability and the tropical cyclone activity over the western north pacific. *Monthly Weather Review* **140**, 140–150 (2012).

50. Cao, X. *et al.* The Projected Poleward Shift of Tropical Cyclogenesis at a Global Scale Under Climate Change in MRI-AGCM3.2H. *Geophysical Research Letters* **51**, e2023GL107189 (2024).

51. Ho, C.-H., Baik, J.-J., Kim, J.-H., Gong, D.-Y. & Sui, C.-H. Interdecadal Changes in Summertime Typhoon Tracks. *J. Climate* **17**, 1767–1776 (2004).

52. Wu, M. C., Chang, W. L. & Leung, W. M. Impacts of El Niño–Southern Oscillation Events on Tropical Cyclone Landfalling Activity in the Western North Pacific. *J. Climate* **17**, 1419–1428 (2004).

53. Liebmann, B., &Hendon, H. H. Synoptic-Scale Disturbances near the Equator. (1990).

54. Timothy J. Dunkerton & Mark P. Baldwin. Observation of 3-6-Day Meridional Wind Oscillations over theTropical Pacific, 1973-1992：Horizontal Structure and Propagation. (1995).

55. Li, T. & Fu, B. Tropical Cyclogenesis Associated with Rossby Wave Energy Dispersion of a Preexisting Typhoon. Part I: Satellite Data Analyses*. *Journal of the Atmospheric Sciences* **63**, 1377–1389 (2006).

56. Li, T., Ge, X., Wang, B. & Zhu, Y. Tropical Cyclogenesis Associated with Rossby Wave Energy Dispersion of a Preexisting Typhoon. Part II: Numerical Simulations*. *Journal of the Atmospheric Sciences* **63**, 1390–1409 (2006).

Acknowledgments

This work is jointly supported by the National Natural Science Foundation of China (Grant 42430611, 42175050, 42275050, 42575186 and 42530605), the Key Laboratory of Polar

Atmosphere-ocean-ice System for Weather and Climate, Ministry of Education (FDAOS-OP202313), the Youth Innovation Promotion Association (CAS Y2021030).

Author contributions

L.W. conceived the study and the interpreting results. R.T.X. processed the data, and wrote the computer code and the initial draft of the paper. Z.Q.G. and Z.P.W. assisted in interpreting results and improve the paper. T.F., X.C. and S.F.C. helped improve the paper. All authors participated in the discussion of results, contributed to manuscript revision, and read and approved the submitted version.

Competing interests

The authors declare no competing financial or non-financial interests.

Fig. 1| Overview of WNP TCs with different disturbance origins, including their proportions, spatial distributions, and composite characteristics. (**a**) Proportion of total WNP TCs (May-Nov, 1981–2020) originating from MRG wave, non-MRG wave, and non-tropical disturbance. (**b**) Genesis density in each 5° × 5° grid for MRG-originated TCs (red), non-MRG-originated TCs (blue), and non-tropical disturbance TC (black). (**c**) Percentage of MRG-originated TCs relative to total TCs (black), along with the number of TCs originating from MRG waves (red), non-MRG-originated (blue), and non-tropical disturbance TC (gray). Dashed lines represent linear trends, with * indicating significance at the 99% level based on the Mann-Kendall trend test. (**d-e**) Composite of MRG-originated TCs at MRG wave time (d) and disturbance (DB) generation time (e), with 2.5-10-day filtered 850-hPa winds (vectors, m/s) and Tb (shading, K). (**f-g**) Composite of MRG-originated TCs at TC generation time (f) and LMI time (g), showing original 850-hPa winds (vectors, m/s) and Tb anomalies (shading, K). (**h-k**) Composite of non-MRG-originated TCs at -24h (h), DB generation time (j), TC generation time (j), and LMI time (k).

Fig. 2| LMI differences among TCs with different disturbance origins in the WNP. (**a**) Differences in LMI (m s^{-1}) among MRG-originated, non-MRG-originated, and non-tropical disturbance TCs in the WNP (May-Nov, 1981–2020). (**b**) Composite difference in 850-hPa horizontal wind (vectors, m s^{-1}) and Tb (shading, K) between MRG-originated and non-MRG-originated at the time of LMI. Vectors and shadings with dots in (b) indicate regions

exceeding the 95% confidence level. (**c**) LMI distribution for MRG-originated (red) and non-MRG-originated (blue) TCs, stars indicate statistical significance at the 95th percentile. (**d**) Annual mean LMI (solid lines) with linear trends (dashed lines) and 95% confidence intervals (shadings) for MRG-originated (red) and non-MRG-originated (blue) TCs.

Fig. 3| Environmental and spatial differences between MRG-originated and non-MRG-originated disturbances in the WNP. (**a**) Standardized density difference of disturbance tracks (MRG minus non-MRG; shaded) on a 2° × 2° grid over the WNP. Plus signs indicate statistical significance at the 95% confidence level. Red and blue dashed lines represent the 1520 gpm contour at 850 hPa, marking the position of the subtropical high ridge during the disturbance periods, respectively. Tracks and genesis points for MRG (non-MRG) disturbances are plotted in red (blue) lines and dots. (**b-g**) Box-and-whisker plots show 20-day low-pass filtered SST (°C), 500-700 hPa mean relative humidity (%), vertical wind shear (m s^{-1}), Tb (K), and divergence at 200 hPa and 850 hPa (10^{-6} s^{-1}), averaged for the MRG region (4°N-16°N, 130°E-180°E) and a non-MRG region (18°N-30°N, 125°E-175°E), based on the density difference sign in (a), during the disturbance lifetime. The mean is shown by the red line, m donating the environmental region's annual average, δ denoting the deviation from the annual average during the disturbance period. Stars at the top left indicate statistical significance at the 95th percentile.

Fig. 4| Evolution and environmental characteristics of MRG-developing disturbance-TC events in the WNP. (**a**) Hovmöller diagram of MRG-developing disturbance-TC events from lag day -1 to +5. Lag day 0 is the developing disturbance genesis time. Shaded area denote MRG-band filtered 850-hPa relative vorticity averaged over 10° S–10° N (10^{-6} s^{-1}); black contours are 2.5-10-day filtered 850-hPa relative vorticity, radial averaging within ±10° of the disturbance center (> 2×10^{-6} s^{-1}). Yellow and green stars mark developing disturbances and TC formation. White, yellow, and green dashed lines denote MRG wave, developing disturbance, and TC track. (**b, c**) Composite MRG and developing disturbance/TC wave at (b) lag day+1 and (c) lag day+3. The red dot indicates the center of the TC. Shaded area denotes MRG-band filtered 850-hPa streamfunction (10^6 m^2 s^{-1}). Black vectors are 2.5-10-day filtered 850-hPa wind (speed > 0.25 m s^{-1}). (**d-i**) Composite environmental fields for MRG and non-MRG-influenced disturbances, showing SST (°C), 500–700-hPa mean relative humidity (rhum; %), vertical wind shear (VWS; m s^{-1}), Tb (K), and 200 and 850-hPa divergence (div; 10^{-6} s^{-1}). Stars at top left denote statistical significance at the 95% level.